**I. Ivanchenko [1], N. Popenko [1],
M. Khruslov [1,2], R. Chernobrovkin [1],
S. Radionov [1], V. Pishchikov [1]**

[1] O.Ya. Usikov Institute for Radiophysics and Electronics of the NAS of Ukraine
12, Acad. Proskura st., Kharkov, 61085, Ukraine
E-mail: buran@ire.kharkov.ua
[2] V.N. Karazin Kharkiv National University
4, Svobody Sq., Kharkiv, 61022, Ukraine

Development of concept of near-field technology in designing effective small-aperture microwave antennas

Subject and purpose. *This article is devoted to the review of the original works of the authors on studying the effective small-sized individual radiators of various types using near-field technology.*

Methods and methodology. *The research algorithm consists in carrying out numerical modeling of the proposed antenna designs using software packages, creating the appropriate physical prototypes and comparing the results of numerical and direct experiments of such radiator characteristics as bandwidth, radiation pattern, gain and ellipticity. At the same time, a detailed analysis of the spatial near-field distributions gives the necessary information for further optimization of the antennas and obtaining their optimal characteristics.*

Results. *The characteristics of various modifications of monopole, disk, aperture, microstrip and spiral antennas with record characteristics are systematized and analyzed, and the possibility of their use in a compact mobile microwave direction finder and nonlinear locator is also shown. The results of studying the diffraction coupling of individual aperture radiators with the involvement of developed methods of measuring the spatial near-field distributions were used to create a laboratory model of an antenna array.*

Conclusions. *A review of the results of studying the small-sized microwave antennas of various types over the past decade is given. We demonstrate the efficiency of using information on the spatial near-field distributions in the inductive and wave regions of the radiating apertures during the elaboration and subsequent optimization of the main characteristics of both individual original radiators and antenna arrays based on them. Fig. 25. Ref.: 59 items.*

Key words: *antenna, antenna array, bandwidth, near-field, radiation pattern.*

The growing demand of wireless services requires the definition of new standards able to provide an increased degree of mobility for the end-user and a higher speed of data transmission. Among emerging standards, one of the most promising is the IEEE 802.16 (WiMax 2 GHz $< f <$ 60 GHz) able to support high-speed wireless broadband applications with rather long reach, mobility, and roaming [1, 2].

A key element here is the antennas of various types. One of the candidates for this purpose is the cylindrical monopole antenna. The advantage of this class of antennas is the ability to produce the different radiation patterns by changing the shape and size of the constituent elements of antennas, including multi-beam radiation patterns [3–5].

The most popular and widely used nowadays are microstrip antennas [6–8]. One of the significant drawbacks of these antennas is their narrow band. In contrast to the microstrip antennas, the dielectric disk antennas (DDA) offer a number of advantages in wireless communication systems due

to low ohmic losses, wider bandwidth etc. [9–11]. With respect to this class of antennas, a special attention is paid to the small-aperture antennas because of the current trend towards the miniaturization of modern devices [12, 13].

As an important task is designing the broadband individual small-aperture radiators and antenna arrays for wireless local area networks, non-destructive control, environmental monitoring, biology, medicine etc. [14–18]. Different techniques related to matching the aperture antenna to its feeding line have been reported in literature, for example by employment of the special air gap [19].

Among the numerous ultra wideband antennas used in the wireless communication systems, a particular attention paid to the planar spiral antennas due to their broadband, high efficiency, low-profile configuration, the stable impedance and circular polarization [20–22]. These antennas are widely used in such applications as direction finding, ground penetrating radar, global positioning systems, in endoscope systems for WBAN in body communications and so on [22, 23]. By taking into account that some applications require the high-performance compact antenna systems, the different techniques are proposed to overcome this problem [22, 24]. The further progress in the practical use of planar spiral antennas operating at frequencies $f > 20$ GHz will be determined by designing the high-performance UWB impedance transformers to match the high input impedance of the spiral antenna with the low impedance feeding line [25–28]. However, the disadvantages of such designs include the fact that in the millimeter range they will have the great losses due to the long feed path. The original planar single-arm fractional spiral antenna with the aforementioned exciting method was reported in [29]. It is worth noting that the variety of practical applications of these antennas sometimes has specific requirements to the feeding or receiving networks, in particular, when the antenna should be loaded with the standard waveguide.

Moving to the higher frequencies, a problem of bearing, for example, the unauthorized local microwave sources becomes a topical question and there is a need of suitable broadband mobile direction finder [30, 31].

In the microwave technology, the aperture radiators based on rectangular waveguides are also both as individual antennas and phased arrays with close packing of elements and wide-angle scanning when operating at high levels of microwave power. In this respect, there is a need to reduce the cross-section of radiators like those. The open ended waveguide filled with a dielectric is usually used as the different transceivers probes or antennas. In this case the problem of waveguide matching with the free space becomes the principle one [32, 33].

The necessity of reducing the antenna apertures results in the most complicated (in terms of the electrodynamics) case when the antenna dimensions become comparable with the operational wavelength. In this respect there is a barest necessity in designing the effective small-aperture microwave antennas to take correctly into account the unavoidable diffraction effects [34]. The main task is to preserve the basic antennas performance. Thereby, the near-field technology becomes one of the main tools [35–37]. This implies the further development and appropriate modification of both the methods for investigating the near-fields in the microwave band and the means for their practical implementation, on which our investigations were focused while designing the original low-aperture microwave antennas and a detailed study of the formation processes of the radiation with the predetermined characteristics.

This review of the original author's works demonstrates the effectiveness of using the near-field technology to create various types of small-sized microwave antennas with optimal characteristics, as well as to study the mutual influence of individual antennas in antenna modules.

1. Cylindrical monopole antennas. The antennas under test consist of the vertical cylindrical monopole as a segment of the central conductor of the coaxial feeding line with a diameter of *2a* (in our investigations $2a = 1.4$ mm) and the circular metal ground plane with the radius R and thickness d (in our case $d = 0.5$ mm) (Fig. 1).

We focus on the two most interesting monopole heights d_{r1}, namely: quarter-wavelength ($d_{r1} = \lambda/4$) and three fourth-wavelength ($d_{r1} = 3\lambda/4$) monopoles for the wavelength $\lambda = 30$ mm. The ground plane radius R varies from 7.5 mm to 82.5 mm with steps of 7.5 mm. Furthermore, the round hole in the ground plane center for coupling with the coax has the radius r which varies from $r = 2.25$ mm, corre-

16

ISSN 1028-821X. Radiofiz. Electron. 2019. Vol. 24, No. 2

sponding to the radius of the coaxial feeding line with the dielectric filling $\varepsilon = 2.04$, to $r = 0.8$ mm. The input reflection coefficient S_{11}, near-field distributions, radiation patterns and antenna bandwidth were selected by us for the analysis. The simulations were performed by using a software package for solving the scattering problems based on the standard finite difference algorithm with the "exact" absorbing conditions on the spherical artificial boundaries in free space and on the transverse artificial boundaries in the feeding line [38]. The measurements were carried out on the experimental equipment [39, 40].

It is quite clear that the most appropriate approach for studying the edge effects caused by the diffraction of EM waves on a finite aperture is the obtaining of information on the spatial distribution of EM fields in the inductive and radiating regions of antenna. There are two typical areas of the edge wave sources, namely, the ground plane edge and the edge of the round central hole in the latter. The interference of these edge waves with the initial wave beam of the monopole will result in the interference picture formation in free space. Therefore, the study of regularities in the interference pictures formation becomes the key aspect allowing one to identify the relationship of the physical parameters of antennas with their radiation pattern shape.

Based on the aforementioned concept, we analyzed the EM field distributions in the inductive region of monopole antennas with the different ground plane radii where the influence of the ground plane size on the antenna beamforming is manifested most clearly [41, 42].

As a result, it has been determined that for the monopole antennas with $d_{r1} = \lambda/4$ two types of spatial near-field distributions depending on the ratio of the ground plane radius and the wavelength is observed. The first type of the EM field distribution has two field variations along the ground plane radius with a minimum, located at a fixed distance from the ground plane edge for antennas with the ground plane radii divisible by $\lambda/2$, and the second one looks like the circular interference picture for antennas with the ground plane radii divisible by odd number of $\lambda/4$. We have called these distributions as the "spatial wave grating". The differences like those explain the oscillating dependencies of both the resonant frequency and the elevation angle of peak directivity. In contrast
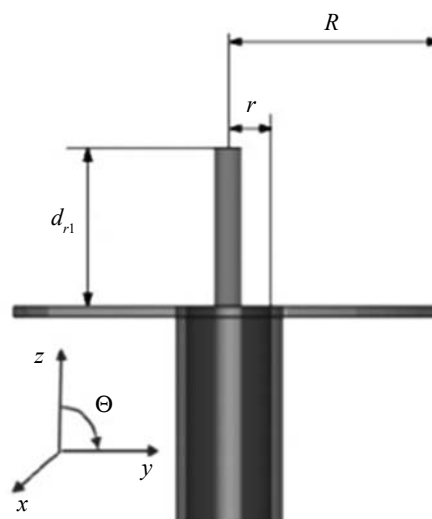

Fig. 1. Schematic view of the antenna

to the antennas with $d_{r1} = \lambda/4$ the resonant frequency and elevation angle of peak directivity for the antennas with $d_{r1} = 3\lambda/4$ are not changed virtually. The thresholds of the ground plane radii of antennas with $d_{r1} = \lambda/4$ and $d_{r1} = 3\lambda/4$ corresponding to the transition from the mono-beam to multi-beam radiation pattern have been defined. Furthermore, and it has been shown that the number of beams increases when increasing the ground plane radius.

We have assumed that for each antenna configuration there is the optimal radius of the round hole in the ground plane center. To confirm this hypothesis, we performed the simulations of cylindrical monopole antennas performance with the monopole heights $d_{r1} = \lambda/4$ and $d_{r1} = 3\lambda/4$ with different radii of the round hole. The minimum value of the return loss coefficient S_{11} was chosen as the criterion of the optimal radius of such a hole for each fixed-sized ground plane.

The comparative analysis of near-field distributions of antennas has showed that the field intensity under the ground plane of the antenna with the monopole height $d_{r1} = 3\lambda/4$ is significantly less than that of the antenna with the monopole height $d_{r1} = \lambda/4$ at the same ground plane radii (Fig. 2). The field intensity on the ground plane edge of the antenna with the monopole height $d_{r1} = \lambda/4$ is 5.7 times higher than that of the antenna with the monopole height $d_{r1} = 3\lambda/4$. In the latter case the EM field distribution is concentrated mainly near the monopole. As a result of this, the contribution of diffraction fields to the antenna beamforming will be much smaller.
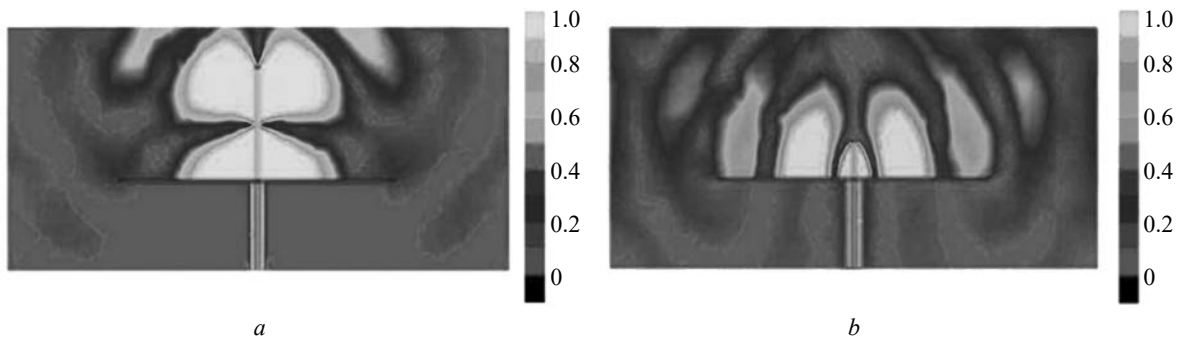
Fig. 2. Near-field distribution of the electric field component E of the antenna with the monopole heights $d_{r1} = 3\lambda/4$ (*a*) and $d_{r1} = \lambda/4$ (*b*) at a fixed time ($R = \lambda = 30$ mm)
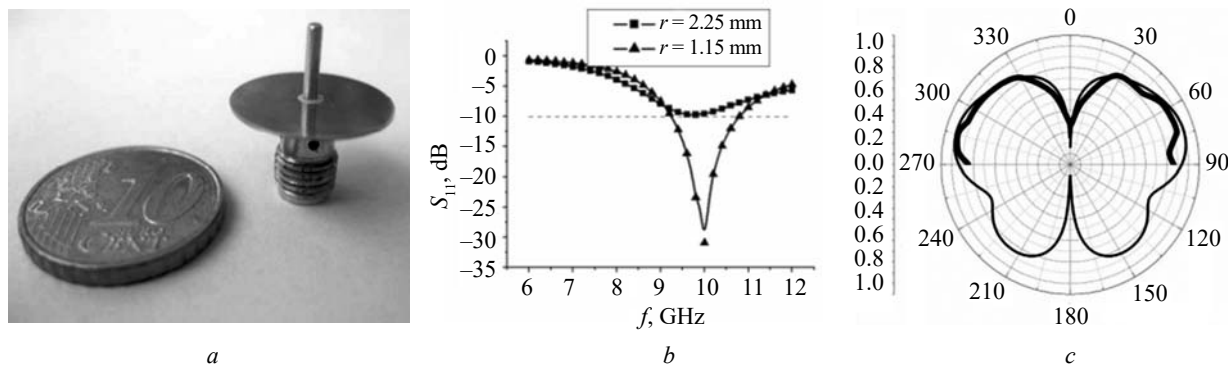

Fig. 3. Antenna prototype (*a*); return loss coefficient S_{11} (*b*); measured (thick line) and simulated (thin line) radiation pattern (*c*) of the antenna with parameters: $d_{r1} = 7.5$ mm, $R = 7.5$ mm, $r = 1.15$ mm

Thus, the optimization of the round hole radius allowed us to design the miniature broadband antenna. The prototype of such the antenna has been manufactured and tested (Fig. 3).

Thus, the physical nature of oscillating dependence of the optimal round hole radius on the ground plane radius of antennas with the monopole height $d_{r1} = \lambda/4$ is explained by different conditions of the formation of spatial near-field distributions in two groups of antennas. We have established the dependence of the optimal round hole radius on the ground plane radius that indicates a validity of the approach applied by us for studying the radiation characteristics of this class of antennas in terms of diffraction-coupled apertures. It has been determined that the variation in the round hole radius of the antenna with a fixed ground plane size results in the resonant frequency shift of the antenna and the antenna efficiency change. It has been established that for each ground plane size of the antenna with the monopole height $d_{r1} = \lambda/4$ one can choose the optimal round hole size at which the antenna performance is maximized. We have also shown that the opti-

mization of the round hole size of the antenna with the monopole height $d_{r1} = 3\lambda/4$ has a meaning only for the ground plane radii $R < 3\lambda/4$.

The choice of the optimal round hole radius allowed us to offer the miniature cylindrical monopole antenna with parameters $d_{r1} = \lambda/4$, $R = 7.5$ mm, and $r = 1.15$ mm which produces a wide-angle mono-beam radiation pattern with the maximum radiation at $\theta = 69°$ in the –10 dB impedance bandwidth BW = 15 %. The antenna seems to be very attractive for using in wireless communications and data transmission such as WiMax.

Computational modelling of the cylindrical monopole antenna with the grounded dielectric layer is also carried out. Notice that the near-field distributions in the inductive region of the given class of antennas are similar to the spatial periodical lattice with different number of variations along the ground radius and with the amplitude decrease to the antenna edge. The calculated antenna characteristics are validated by measurements on the antenna prototypes [43–45].

2. Dielectric disk antennas. The dielectric disk antennas (DDA) are positioned as the cheapest

class of antennas that require a little time to develop and manufacture. As well-known, the conical radiation pattern is characteristic for these antennas. At the same time, the functionality of the DDA can be extended, for example, by providing their axial radiation. The easiest way to get the radiation pattern with a radiation maximum oriented in the antenna axis is an off-axis excitation of such a structure.

The cylindrical DDA consisting of a dielectric disk ($\varepsilon = 10$) of height h and radius a, located on a dielectric substrate ($\varepsilon = 1.18$) of height h_{sub} located above the ground plane was selected as a model for studying (Fig. 4). The radii of the substrate and the ground plane coincide with the disk radius a. The excitation is realized by the monopole of height l_s, displaced along the disk radius at the distance l_x from the radiator axis [46].

Numerical modeling was performed by using the software package Ansoft HFSS. During the numerical simulations the geometric parameters of the DDA such as h, a, h_{sub}, l_s, l_x were changed. As a result of that the following dimensions of the radiator, for which the return loss coefficient is minimal, were determined, namely: $h = 2.5$ mm, $a = 10$ mm, $h_{sub} = 2.5$ mm, $l_s = 3$ mm, $l_x = 4.5$ mm. We calculated the characteristics of the proposed DDA such as the radiation pattern, gain, return loss coefficient (S_{11}), and the amplitude distribution of the electric component in the near-field of the radiator.

As an example, the near-field distributions for the optimal and non-optimal height of the feeding monopole have been shown in Fig. 5. The monopole height $l_s = 3$ mm providing the minimal value of the return loss coefficient was chosen as an optimal. In this case the axially symmetric EM field distribution is observed, but the center part of the near-field distribution is shifted relative to the DDA center away from the feeding monopole (Fig. 5, *b*).

It is revealed that the maximum contribution to radiation comes from leaky waves from the side faces located on the monopole side. (Fig. 5, *a*). At the optimum position of the feeding monopole $l_x = 4.5$ mm the field distribution becomes symmetric (Fig. 5, *b*). Such an antenna has an axially-symmetric mono-beam radiation pattern with the back-lobes level −6 dB. The beamwidth of the radiation pattern in the *E*-plane is 75°, and in the
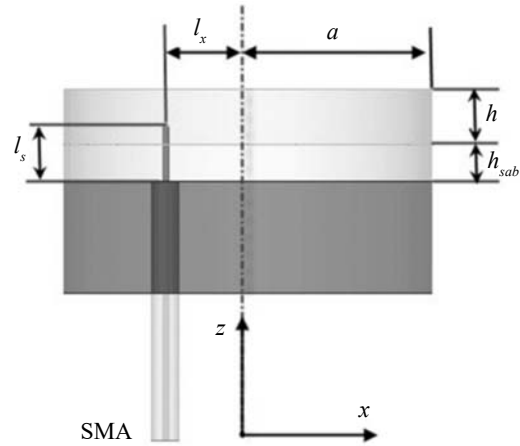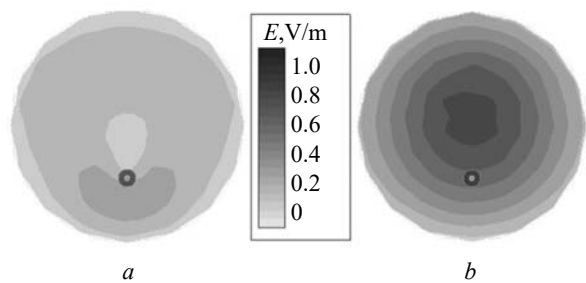

Fig. 4. DDA with off-axis excitation

Fig. 5. Near-field distribution of the DDA for two heights of the monopole: *a* – $l_s = 2.5$ mm; *b* – $l_s = 3$ mm
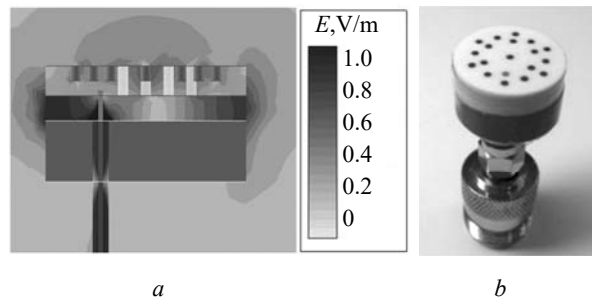

Fig. 6. Simulated near-field distribution at $f = 7.5$ GHz (*a*) and DDA prototype (*b*)

H-plane is 90°, that is caused by the asymmetric near-field distribution. The radiation pattern retains the shape in the operational frequency band. The maximum gain is 6 dBi. However, the asymmetric near-field distribution relative to the DDA axis leads to shifting the elevation angle of peak directivity of 5° relative to the radiator axis. From the point of view of designing the radiator with a narrower radiation pattern and the radiation maximum oriented in the zenith, it was suggested to adjust the amplitude-phase distribution at the DDA aperture by introducing the additional passive dipoles (Fig. 6, *a*) [47].
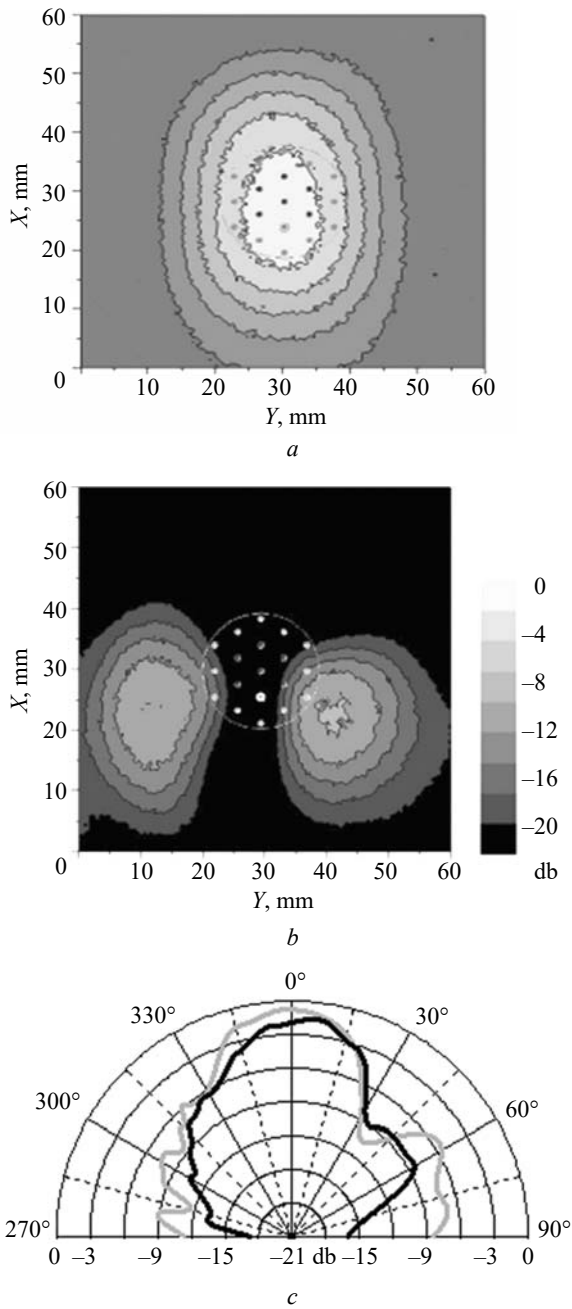
a

b

c

Fig. 7. Measured near-field distributions of the DDA at the frequency f = 7.8 GHz: (*a*) E_x-component; (*b*) E_y-component and the radiation pattern (*c*) (gray line belongs to the *E*-plane, and black line belongs to the *H*-plane)
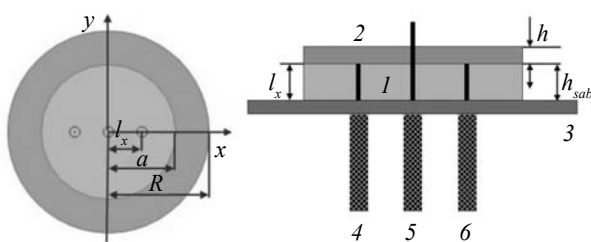

Fig. 8. Schematic view of the antenna

Based on the data obtained in simulations, the DDA prototype with the metalized dielectric disk has been manufactured (Fig. 6, *b*). We measured the return loss coefficient, near-field distribution and radiation pattern of the prototype. The near-field distributions for the E_x and E_y components are shown in Fig. 7, *a*, *b*.

The radiation patterns of the DDA measured in the *E*- and *H*-planes are shown in Fig. 7, *c*. The beamwidths in the *H*- and *E*-planes are 28° and 40°, respectively. Herewith, the elevation angle of peak directivity coincides with the radiator axis.

With the aim to further extending the functionality of DDA based devices the idea of implementing a two-mode operation with the possibility of consistent forming the alternating fundamentally different radiation patterns seems to be very attractive. We have proposed a small-aperture DDA being capable of generating two different radiation patterns [48].

The antenna consists of two dielectric disks *1* and substrate *2* with relative permittivity 9.8 and 1.18 respectively located on the metallic ground plane *3* (Fig. 8).

In order to provide the antenna operation in two modes with different radiation patterns having a maximum and a minimum of radiation in the axial direction of the antenna, we have applied three identical monopoles two of which (*4* and *5*) are active and one *6* is passive. All monopoles are located on the same line. The monopole *4* is located close to the antenna edge and serves to form the radiation pattern with the radiation maximum in the antenna axis. The monopole *5* is located in the antenna center providing the omnidirectional conical radiation pattern with the characteristic radiation minimum in the antenna axis. The passive monopole *6* is located symmetrically with respect to the monopole *4*. The monopole *6* serves to provide the necessary amplitude and phase spatial distributions on the antenna aperture.

In simulations the geometric parameters of DDA were changed within the following limits: the radius of dielectric disks 8 mm < *a* < 12 mm; the height of dielectric disks 1 mm < *h* < 5 mm and 1 mm < h_{sub} < 4 mm, respectively; the ground plane radius 10 < *R* < 25; the distance between monopoles *4* and *5* (as well as between monopoles *6* and *5*) 4 mm < l_x < 12 mm. By analyzing the results of simulations, the antenna with the radi-

20

ISSN 1028-821X. Radiofiz. Electron. 2019. Vol. 24, No. 2
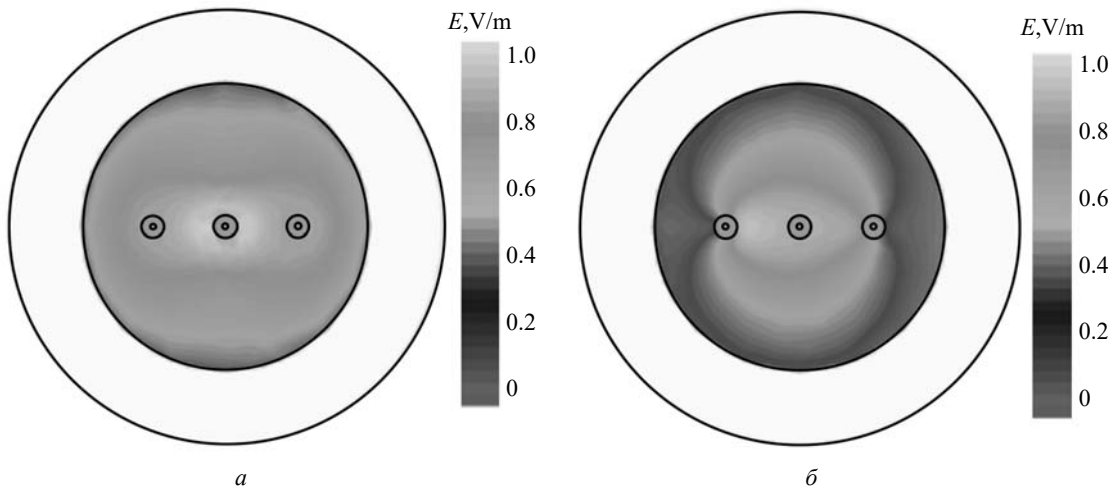
Fig. 9. Near-field distributions of the antenna excited by the monopole *4* (*a*) and monopole *5* (*b*)

us *a* = 10 mm of both dielectric disks has been chosen because just in this case the resonant frequencies are closest, the appropriate S parameters are less than –16 dB for both operational modes of the antenna, and the –10 dB impedance bandwidth is 20 %. By analyzing the near-field distributions on the antenna aperture depending on the relative position $2l_x$ of monopoles *4* and *6*, it was found the matching of antenna with a feeding line is improved when these monopoles move to the dielectric disk edge. At the same time, the symmetrical near-field distribution is achieved when the active monopole *4* is located on the distance $a/2$ (for $2l_x$ = 10 mm*)* (Fig. 9, *a*). We can also see the symmetrical near-field distribution (Fig. 9, *b*) in the case of the active monopole *5*.

The antenna prototype with optimal parameters noted above was manufactured (Fig. 10).

The antenna is able to operate in two modes corresponding to different radiation pattern shapes, namely: with the angle of peak directivity in the antenna axis and with the minimum radiation power (the level less than –21 dB) in the antenna axis. It can be used in different wireless communication systems, for instance, as a primary source of the reflector antenna.

3. Direction finder. We have proposed a compact broadband microwave direction finder, the principle of which is based on using the "zero amplitude" method. The direction finder antenna contains a main parabolic reflector with an aperture radius of 80 mm and a primary source located at the focus of the reflector. The main feature of the an-

Fig. 10. The antenna prototype

tenna is the use of a primary source in the form of a cylindrical monopole antenna [49–51]. In order to study the process of forming the radiation of a reflector antenna and optimize the relative position of its component elements, we have carried out a preliminary simulation of such an antenna. As a result, the optimal dimensions of the monopole and the ground plane were determined (the height of the monopole and the radius of the ground plane are 22.5 mm), in terms of the reflector blockage

and the utilization factor of its surface. The simulation results obtained were used to create a physical prototype of the direction finder, the appearance of which is shown in Fig. 11, *a*.

Fig. 11, *b* shows the measured distribution of the near-field of the antenna at a frequency *f* = 10 GHz. As can be seen from the figure above, there is one main lobe and a weak side lobe at a level of about –15 dB.
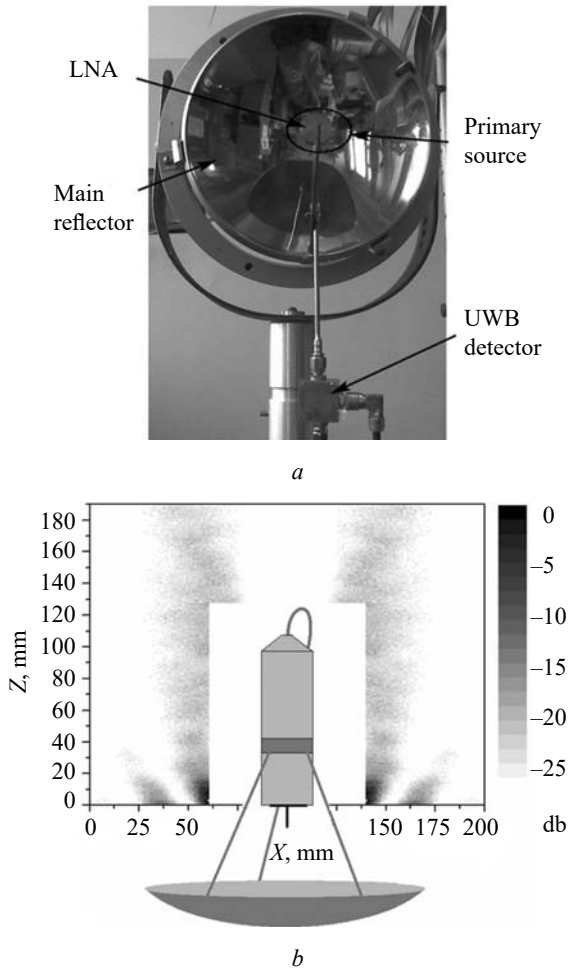
To implement the signal reception mode, we have integrated a three-stage HEMT-based amplifier into the circuit, which allows us to achieve a noise-factor not worse than 0.5 dB within the operational frequency band. The fabricated and optimized reflector antenna forms the mono-beam conic radiation pattern in the 6–11 GHz frequency band with the elevation angle of the peak directivity θ = 10° (Fig. 12, *a*).

The level of side lobes does not exceed –20 dB. The bearing process is simulated on the front panel of the control unit (Fig. 12, *b*) by means of the appropriate arrangement of the LEDs, each pair of which corresponds to a certain level of the received signal.

By using the developed algorithm, we have showed that a direction on the sought-for microwave source can be determined with evaluation accuracy of 1.5°.

4. Microstrip antennas. The microstrip antennas are first of all considered to operate at mobile communication frequencies. The main requirements for such antennas are as follows: small dimensions and weight, low-profile, low cost, good matching and high gain. However, the use of multi-frequency antennas can be extended to studying the nonlinear processes. In this way, the main problem will be to study the radiation characteristics of the antenna at higher harmonics that can arise, for example, as the result of interaction of the electromagnetic radiation with a nonlinear medium under test. In this case, the operational frequencies of the antennas should differ by a factor of two and the realization of these conditions can be ensured by the creation of an antenna module comprising at least two antennas operating on two lower harmonics of the microwave signal. When creating such an antenna module, it is necessary to ensure not only good matching and high gain of each antenna, but also a
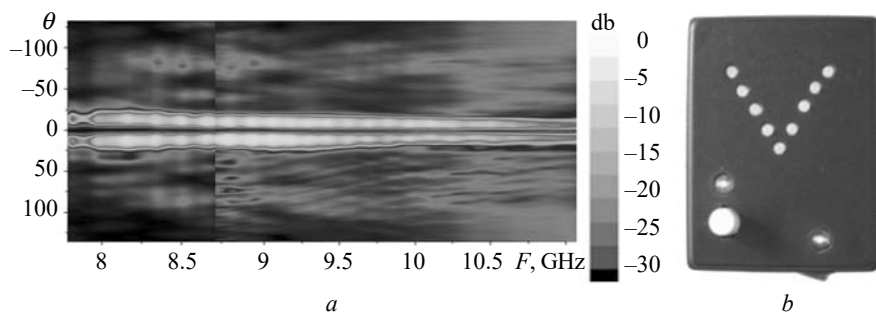

Fig. 11. Direction finder prototype (*a*) and measured near-field distribution (*b*)

Fig. 12. Radiation pattern of the reflector antenna (*a*) and control unit (*b*)
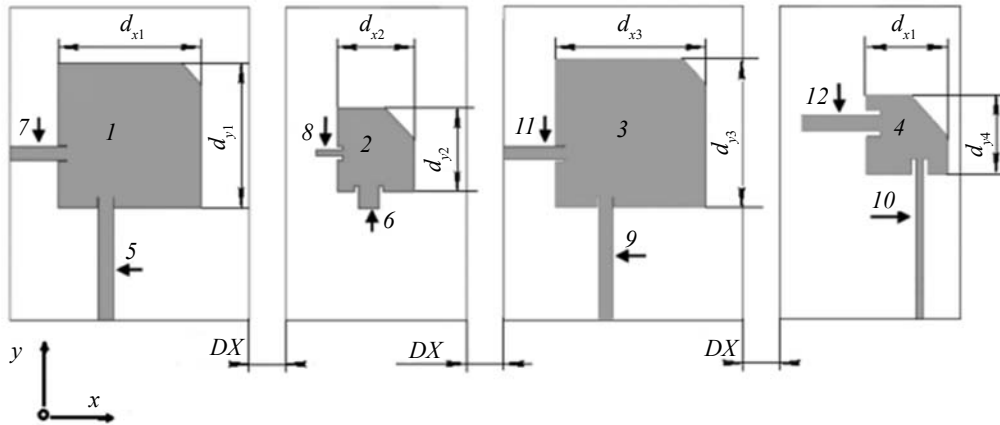
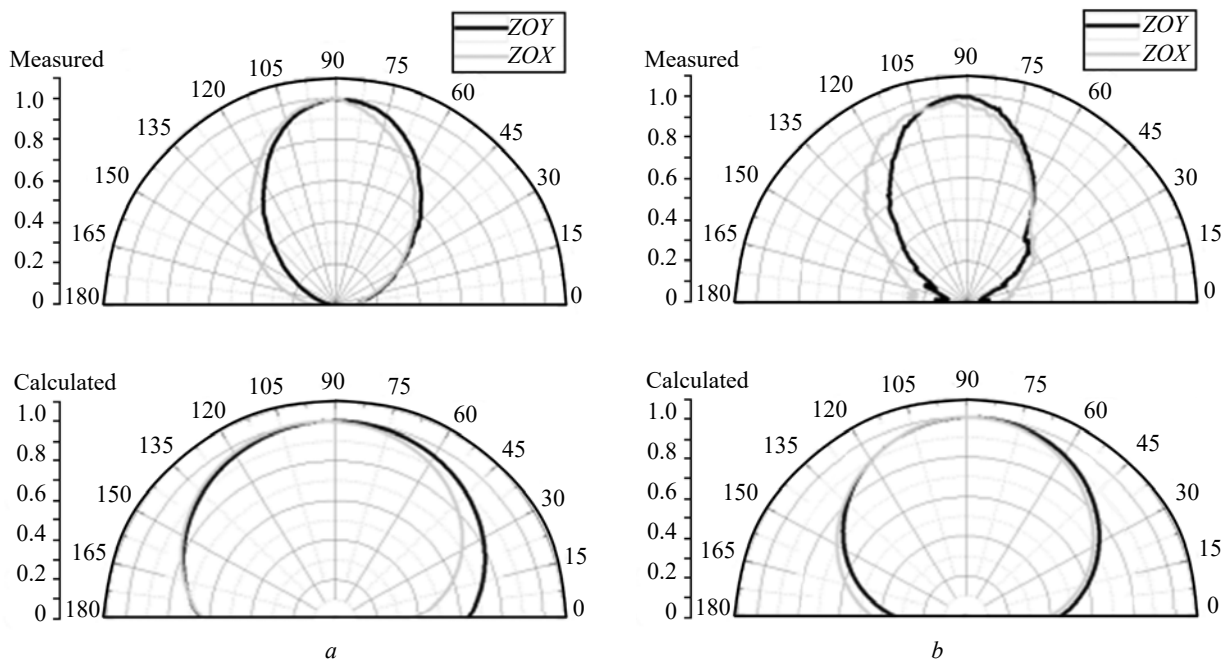***Fig. 13.*** Geometry of the antenna module

Fig. 14. Calculated and measured radiation patterns of antennas *1* (*a*) and *2* (*b*) in two principal planes

good isolation between them. Herewith, it should be kept in mind that coupling between the antenna apertures can occur due to the influence of the radiation from one antenna on the characteristics of the other antenna, and also due to waves arising in the substrate. To ensure high measurements sensitivity, it must be borne in mind that the "parasitic" signal magnitude on both antennas should be less than –50 dB. To increase the sensitivity of such an antenna module, the super heterodyne circuit of measurements seems most appropriate. Thereby, the additional pair of antennas operating at the appropriate frequencies we proposed to use in the antenna module (Fig. 13) [52].

The radiation patterns in both principal planes are shown in Fig. 14. Notice that the calculated and measured elevation angles of peak directivity are close to zenith for all antennas. Herewith, the measured radiation patterns are narrower than the calculated ones and their beamwidths are in the interval of angles $64° ≤ ΔΘ ≤ 68°$. It is especially important that the side lobes level does not exceed –20 dB.

To analyze the effect of each of the antennas on others, the near-field measurements were carried. Since the results of of near-field measurements of any two adjacent antennas are practically repeated, we confine ourselves to a representation of the
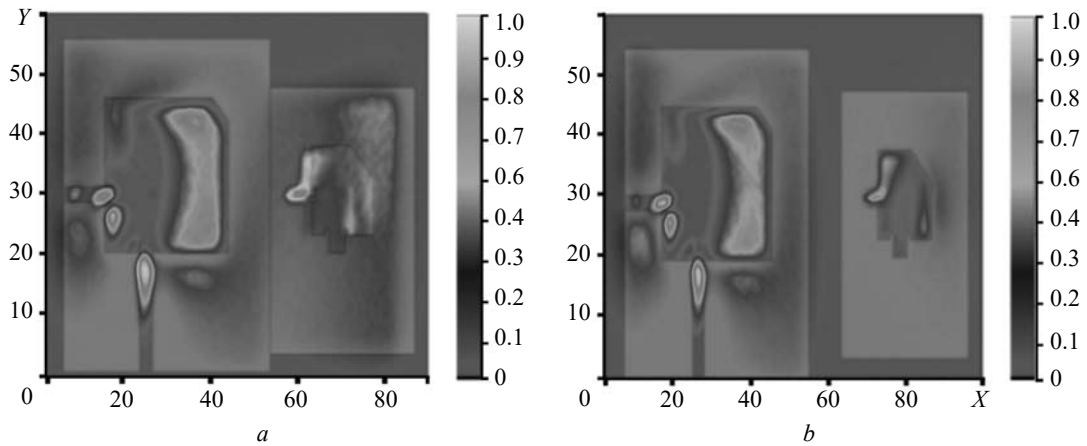
Fig. 15. Measured near-field distributions when both antennas radiate simultaneously: $DX = 0$ mm (*a*), $DX = 13$ mm (*b*)

field pictures of two antennas, in particular, of antennas *1* and *2* (see Fig. 13). The measurements were carried out in the inductive region by a magnetic dipole for different widths of the gap *DX*.

Based on the measured frequency dependences of S_{12} parameter we have revieled that the latter decreases when the gap increases and for $DX > 13$ mm the parameter S_{12} becomes < -50 dB that is already an acceptable value from the point of view of realization of the aforementioned goal. The typical near-field distributions are shown in Fig. 15.

So, the minimum permissible distance between the antennas has been determined, at which the operation of each of antennas is not affected by the operation of other antennas, i.e., they are electromagnetically independent.

5. Spiral antennas. The most typical feature of the spiral antennas is a high input resistance. Therefore, a good matching of feeding 50-Ω coaxial cable with the antenna in the wide frequency band becomes a major problem. Herewith, a wideband antenna operation is archived by using the different designs of transformers (baluns). In our study, we propose to apply the wideband conical transition as an impedance transformer network in the feeding section of the spiral antenna [53]. Schematic view of the transformer is shown in Fig. 16.

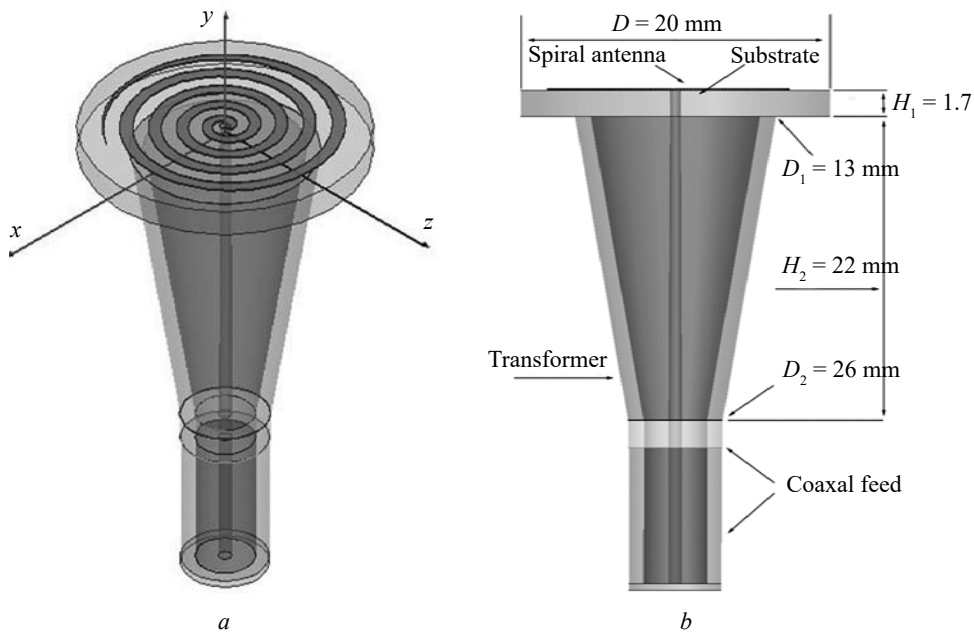The transformer represents a truncated hollow metal cone filled with the dielectric. In simulations,

**Fig. 16.** Shematic views of the antenna: 3D picture (*a*), plot of the transformer (*b*)

24

ISSN 1028-821X. Radiofiz. Electron. 2019. Vol. 24, No. 2

the height H_2 of the cone, diameter D_1 of the bigger cone base, and relative dielectric permittivity of transformer filling e_t varied within the following limits: 5 mm < H_2 < 45 mm; 5 mm < D_1 < 15 mm; 2.04 < e_t < 3.8. Cross-section of the smaller cone base has the diameter D_2 and corresponds to the cross-section of the feeding coaxial cable. Following the simulations, the input reflection coefficient is S_{11} < 10 dB through the frequency band from 7.5 GHz to 45 GHz. The antenna demonstrates a mono-beam radiation pattern within the operational frequency band. We note that the beamwidth decreases when moving toward higher frequencies because of increasing the relation of the antenna diameter and wavelength. As an example, we give the near-field distributions in the inductive region of the antenna (Fig. 17, *a*). The field pictures point out a maximum of the field intensity in the area of antenna center with the gradual decrease in the field intensity to the antenna edges. As one sees from these pictures the EM field distribution looks like to be a sufficiently homogeneous one close to the antenna center at all frequencies. If the operational frequency increases the space area with a high intensity of the EM field slightly moves on the antenna surface.

In according to the simulated results, the antenna prototype has been manufactured and tested (Fig. 17, *b*). The measurement results are in good agreement with simulations.

In contrast to the conventional excitation of the spiral antenna by means of microstrip line, we have offered for the first time the compact planar spiral antenna with a feeding network as the standard rectangular waveguide for the wireless applications in the long-wave region of the millimeter range. Schematic view of the antenna is shown in the Fig. 18, *a*. Following the results of simulations, the optimal physical and geometric parameters of this complicated structure have been determined. The prototype of such antenna module was elaborated and tested (Fig. 18, *b*) [54].

As an example, the measured near-field distributions for the E_y-polarization are shown in Fig. 19.

The return loss coefficient of the antenna points out the –10 dB impedance bandwidth from 32 GHz to 38 GHz. The measured axial ration does not exceed –3 dB in the frequency band 32–36.5 GHz. The differences in the radiation pattern shapes for two orthogonal polarizations and the axial ration
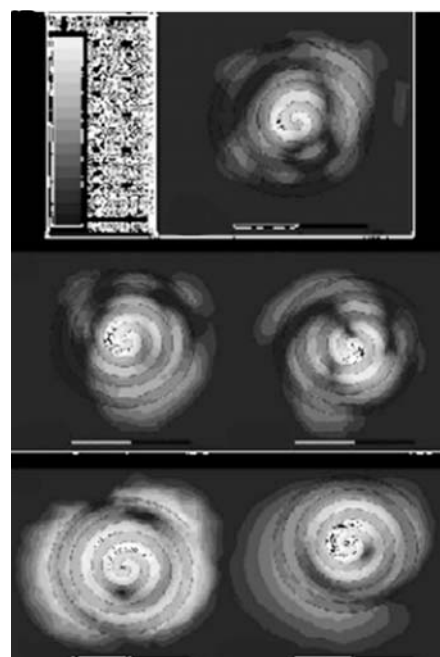
a
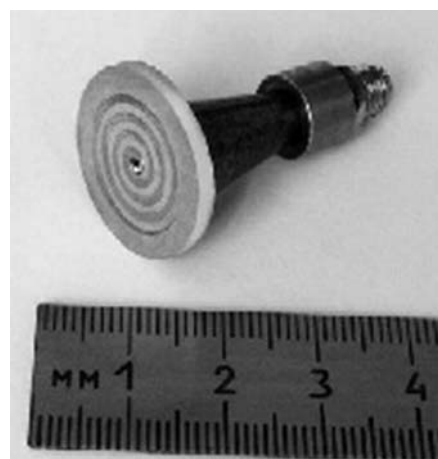
b

Fig. 17. Near-field distributions of the spiral antenna (*a*), antenna prototype (*b*)

changing, and the nature of their changing in the limits of antenna bandwidth become apparent following the analysis of measured near-field distributions. The proposed antenna can be used for different practical applications in the long-wave region of millimeter range.

Moving towards the higher frequencies the disadvantages of such designs include the fact that in the millimeter range they have the great losses due to the long feed path. In this regard, we proposed two original planar single-arm fractional spiral antennas with circular polarization and different radiation patterns (Fig. 20) [55].
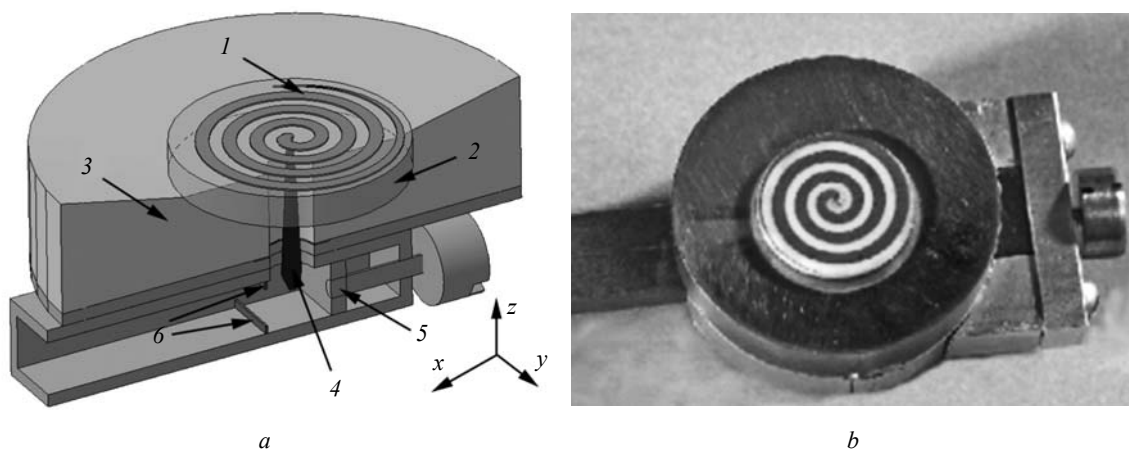
Fig. 18. Schematic view of the antenna module (*a*): *1* – spiral antenna; *2* – substrate; *3* – spherical metal mirror; *4* – feeding line; *5* – shorting piston; *6* – metal diaphragms; general view of the antenna prototype (*b*)
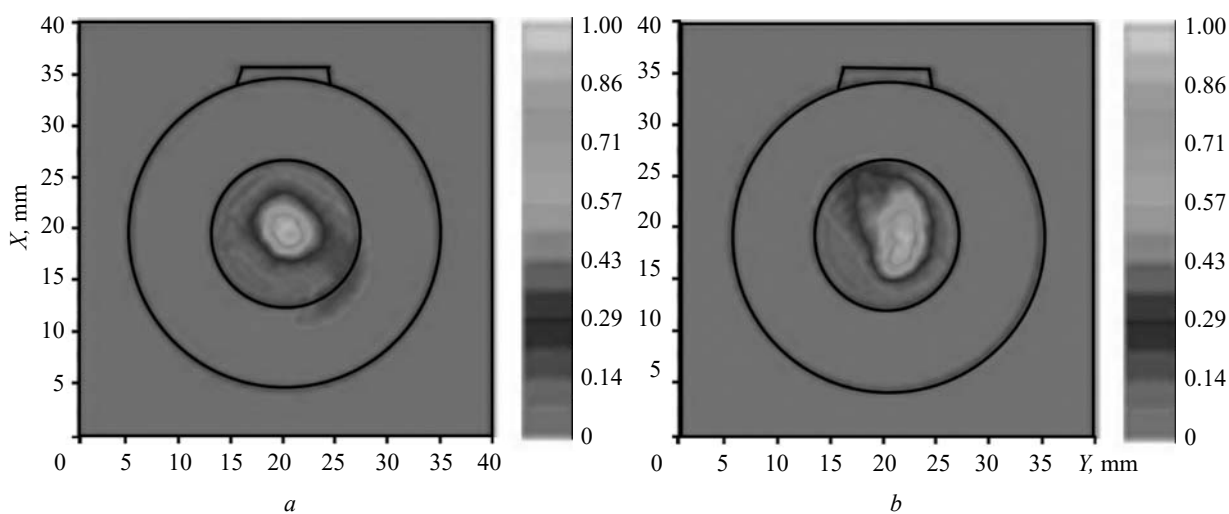

Fig. 19. Near-field distributions: *f* = 32.08 GHz (*a*); *f* = 37.76 GHz (*b*)
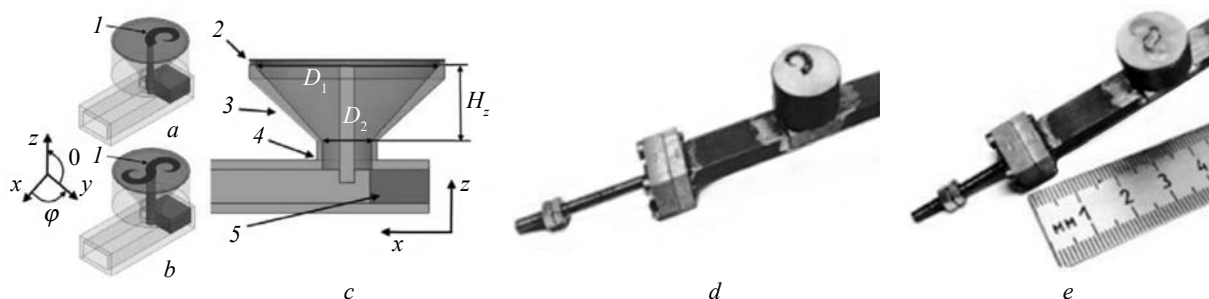
Fig. 20. Geometry of the antennas: single planar spiral (*a*), double planar spiral (*b*), antenna loaded with the waveguide (*c*). Two antenna prototypes: single planar spiral (*d*), double planar spiral (*e*)

The influence of edge effects as well as impedance matching of the antenna input with the feeding line on the antenna performance can be studied by applying near-field technology. As an illustra-tion, the near-field distributions for the double planar spiral antenna is shown in Fig. 21. Near-field distributions were measured in the *XOY*-plane, when the vector *E* of the probe was oriented along

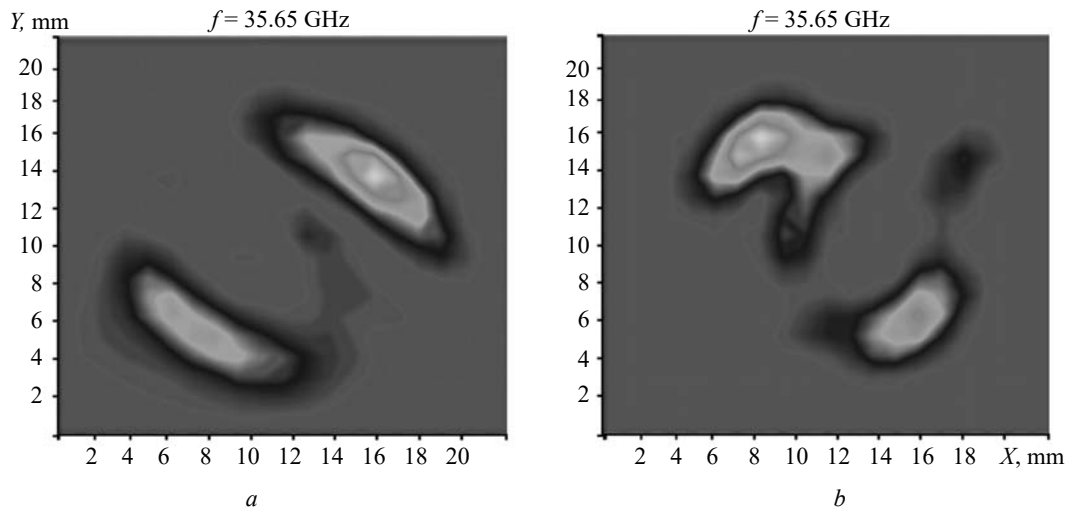**Fig. 21.** Measured near-field distributions of the double planar spiral antenna in the *XOY*-plane when the vector *E* of the probe was oriented along *OX*-axis (Fig. 11, *a*) and *OY*-axis (Fig. 11, *b*)
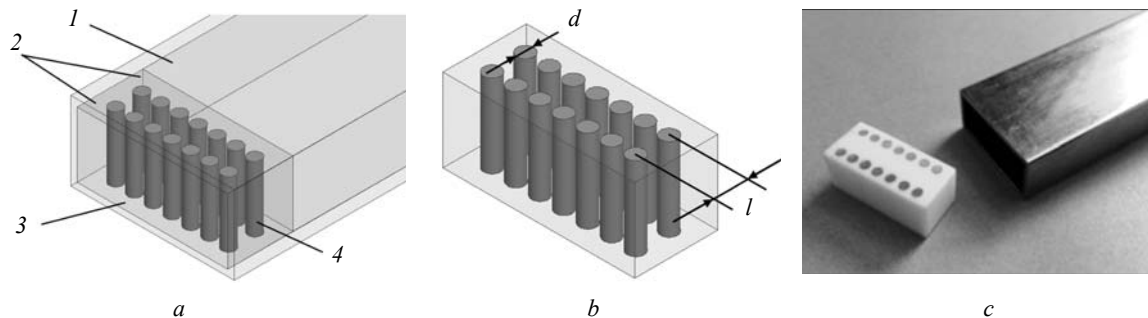

Fig. 22. General view of the open ended waveguide (*a*), the configuration of dielectric insertion (*b*), and photo of the antenna elements (*c*)

OX-axis (Fig. 11, *a*) and *OY*-axis (Fig. 11, *b*), respectively. The field pictures obtained are characteristic for this antenna with a circular polarization.

As the result, the measured return loss coefficients point out the –10 dB impedance bandwidth of 6.12 GHz and 5.93 GHz for the single and double planar spiral antennas respectively. The radiation pattern of the single spiral antenna is characterized by the wide lobe with the elevation angle of peak directivity near the antenna axis. For the double spiral antenna, we obtained the omnidirectional radiation pattern in the azimuth plane with the elevation angle of peak directivity oriented at $\theta_{max} = \pm 20°$ and with the minimum intensity in the antenna axis. The axial ration does not exceed –3 dB in the frequency band *f* = 32–38.8 GHz for the single spiral antenna and *f* = 32.4–37.1 GHz for the double spiral antenna.

6. Aperture antennas. The open ended waveguide filled with a dielectric is usually used as the

different transceivers probes or antennas. It is quite clear that the problem of waveguide matching with the free space becomes the principle one. We have proposed the antenna as the open-ended waveguide filled with the metamaterial analogue that allows for forming the various near-field distributions on the radiator aperture by means of definite combinations of the local inhomogeneities inside the Teflon matrix [56].

Antenna under test is an open-ended waveguide *1* with the hybrid dielectric insert *2* inside, which is a lattice of dielectric cylinders *3* in the dielectric matrix *4* (Fig. 22, *a*). The cross-section of the dielectric matrix corresponds to the cross-section of the waveguide. Dielectric cylinders of diameter *d* form the double-row lattice with the period *l* (Fig. 22, *b*). Herewith, the permittivity of the cylinders and the matrix differ from each other.

A number of antenna designs with different lattice topology were analyzed. Some of them have

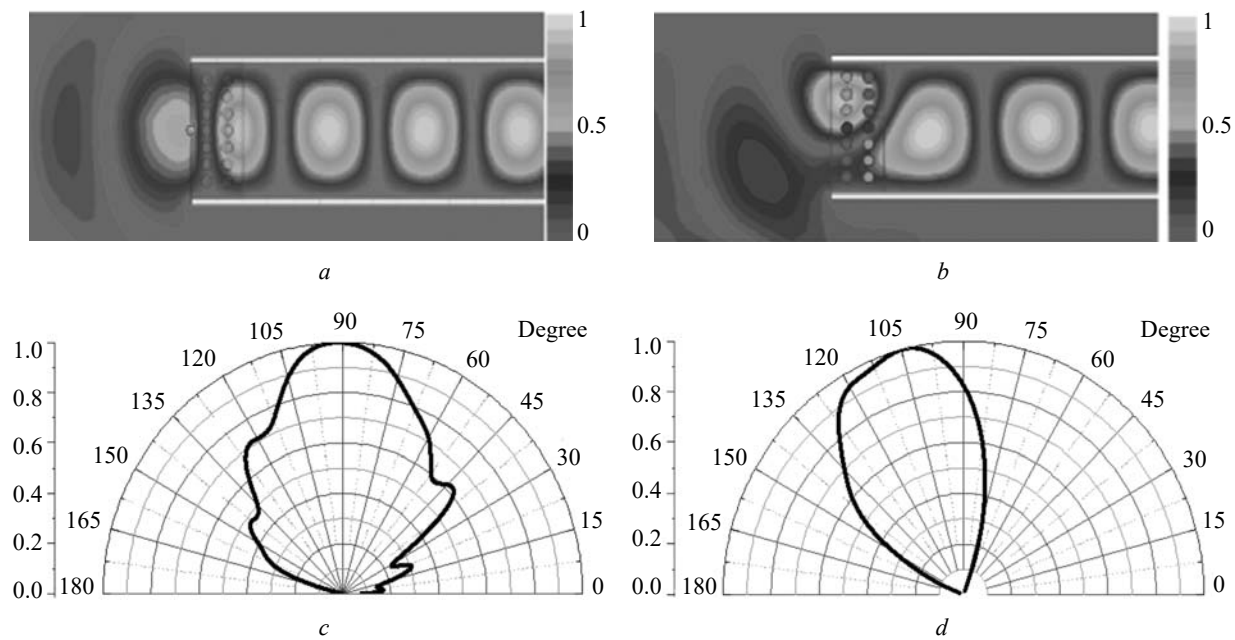**Fig. 23.** Near-field distributions (*a*, *b*) and radiation patterns in the *E*- (*c*) and *H*-planes (*d*) at f_r = 9.8 GHz
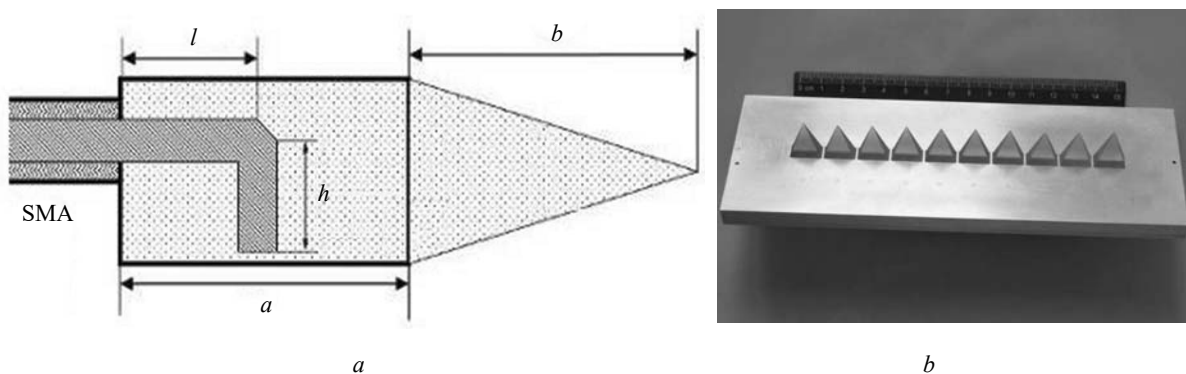

Fig. 24. Design of the individual radiator (*a*) and linear array prototype (*b*)
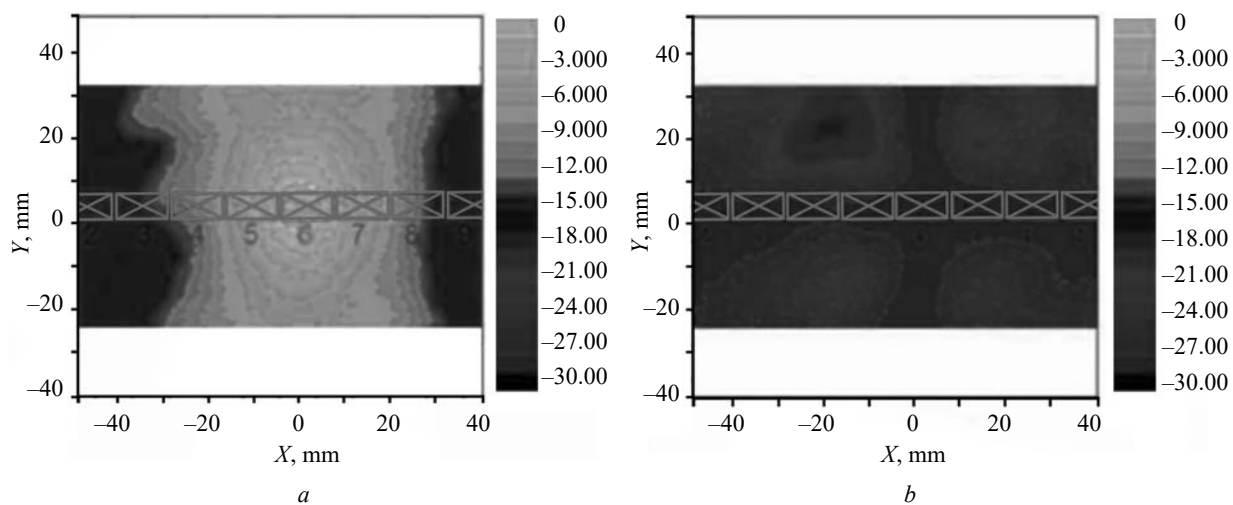

Fig. 25. Near-field distributions of the center element of the array at 8.45 GHz; *a* – co-polarization, *b* – cross-polarization

28

ISSN 1028-821X. Radiofiz. Electron. 2019. Vol. 24, No. 2

been manufactured and tested in the frequency band 8–12 GHz. We have showed the possibility to control the near-field distributions and hence the antenna performance by means of definite combinations of the dielectric cylinders with different permittivity (air and quartz) which are oriented parallel to the vector *E* of the operational waveguide mode (Fig. 23).

It was shown that when using cylinders with the same dielectric constant (Fig. 23, *a*), the elevation angle of peak directivity of such an antenna in both principal planes is oriented in zenith. At the same time, by using the cylinders with different permittivity and by combining them differently in the lattice (Fig. 23, *b*), the elevation angle of peak directivity can change in the *H*-plane (Fig. 23, *d*).

7. Antenna array. A set of original probe designs as the open-ended waveguide filled with a dielectric was proposed which were used for near-field measurements in the radiating region of radiated apertures [57–59]. Some of them have been applied as the individual radiator in antenna arrays to provide the space between the elements in the X-band antenna array less than half a wavelength. One of the novelties of the individual radiator is a transition from SMA connector to waveguide using an original excitation pin (Fig. 24, *a*) [58].

Based on our results of theoretical and experimental investigations we manufactured the linear array prototype, depicted in Fig. 24, *b*. The antenna array consists of 10 radiators located at a mutual distance of 15 mm. The aggregate length of the antenna amounts 30 mm. We have measured and analyzed the EM field distributions in the radiating region of each elementary radiator integrated in the antenna array. Co- and cross-polarizations per element have been investigated by having all other radiators terminated with matched loads.

As an example, the near-field distributions of radiators are shown in Fig. 25.

The scanning angle of the antenna array is around ±50° and the side lobes level does not exceed –9 dB.

Conclusions. A review of results of our investigations related to the small-sized microwave antennas of various types over the past decade is given. The efficiency of using the information on the spatial distribution of fields in the inductive and wave regions of the radiating apertures has been demonstrated at designing and subsequent optimization of the characteristics of both individual original radiators and antenna arrays comprising such the radiators.

REFERENCES

1. Kim, T., Park, D., 2005. CPW-fed compact monopole antenna for dual-band WLAN applications. *Electron. Lett.*, 41(6), pp. 291–293.
2. Wong, K., Su, W., Chang, F., 2006. Wideband internal folded planar monopole antenna for UMTS/WiMAX folder-type mobile phone. *Microwave Opt. Technol. Lett.*, 48(2), pp. 324–327.
3. Chun, J.C., Shim, J.R., Kim, T.S., 2007. Wideband cylindrical monopole antenna for multi-band wireless applications. In: *Proc. Int. Antennas and Propagation Society Symp.* Honolulu, Hawai'i, USA, 9–15 June 2007, pp. 4749–4752.
4. Jong-Ho, J., Park, I., 2003. Electromagnetically coupled small broadband monopole antenna. *IEEE Antennas Wirel. Propag. Lett.*, **2**(1), pp. 349–351.
5. Guha, D., Ganguly, G., Sumesh, G., Kumar, Ch., Sebastian, M., Antar, Ya., 2017. A New Design Approach for a Hybrid Monopole to Achieve Increased Ultrawide Bandwidth. *IEEE Antennas Propag. Mag.*, **59**(1), pp. 139–144.
6. Roy, A., Anand, S., Choudhury, P., Sarkar, P., Bhunia, S., 2014. Compact Multi Frequency ApproachPatch Antenna with Spur-Lines for WLAN/WIMAX Applications. *Int. J. Electron. Commun. Technol.* (IJECT), **5**(2), pp. 84–86.
7. Das, S., Bhattacharjee, A., Sarkar, P., Chowdhury, S., 2013. Reduced Size Multifrequency Microstrip Patch Antenna for Wireless Communication Applications. *Int. J. Electron. Commun. Technol.* (IJECT), **4**(5), pp. 26–28.
8. Mingming, G., 2015. The Microstrip Antenna Design for Multiple Frequency Small Broadband. In: *Int. Conf. Intelligent Systems Research and Mechatronics Engineering.* (ISRME 2015). Proc. Zhengzhou, China, 11–13 April 2015, pp. 2159–2162.
9. Kishk, A., Zunoubi, M., Kajfez, D., 1993. A Numerical Study of a Dielectric Disk Antenna Above Grounded Dielectric Substrate. *IEEE Trans. Antennas Propag.*, **41**(6), pp. 813–821.
10. Huang, W., Kishk, A., 2007. Compact Wideband Multi-Layer Cylindrical Dielectric Resonator Antennas. *IET Microwaves Antennas Propag.*, **1**(5), pp. 998–1005.
11. Kishk, A., 2003. Wide-Band Truncated Tetrahedron Dielectric Resonator Antenna Excited by a Coaxial Probe. *IEEE Trans. Antennas Propag.*, **51**(10), pp. 2913–2917.
12. Petosa, A., Ittipiboon, A., 2010. Dielectric Resonator Antennas: A Historical Review and the Current State of the Art. *IEEE Antennas Propag. Mag.*, **52**(5), pp. 91–116.
13. Kishk, A., Huang, W., 2011. Size-Reduction Method for Dielectric Resonator Antennas. *IEEE Antennas Propag. Mag.*, **53**(2), pp. 26–38.

14. Li, R., Thompson, D., Papapolymerou, J., Laskar, J. and Tentzeris, M.M., 2005. A new excitation technique for wide-band short backfire antennas. *IEEE Trans. Antennas Propag.*, **53**(7), pp. 2313–2320.

15. Kuo, Y., Wong, K., 2003. Printed double -T monopole antenna for 2.4/5.2 GHz dual-band WLAN operations. *IEEE Trans. Antennas Propag.*, **51**(9), pp. 2187–2192.

16. Chen, H-D., Chen, H-T., 2004. A CPW-Fed dual-frequency monopole antenna. *IEEE Trans. Antennas Propag.*, **52**(4), pp. 978–982.

17. Nakano, H., Ikeda, N., Wu, Y-Y., et al., 1998. Realization of dual-frequency and wide-band VSWR performances using normal-mode helical and inverted-F antennas. *IEEE Trans. Antennas Propag.*, **46**(6), pp. 788–793.

18. Baudry, D., 2007. Applications of the Near-Field Techniques in EMC Investigations, Electromagnetic Compatibility. *IEEE Trans. Electromagn. Compat.*, **49**(3), pp. 485–493.

19. Coman, C.I., Lager, I.E., Ligthart, L.P., 2004. The Design of a Matching Circuit for Dielectric-filled Open-ended Waveguide Antenna. In: *Proc. European Radar Conf.* (EuMW'2004). Amsterdam, Netherlands, 11–15 October 2004, pp. 73–76.

20. Thaysen, J., Jakobsen, K., Appel-Hansen, J., 2001. A Logarithmic Spiral Antenna for 0.4 to 3.8 GHz. *Appl. Microwave Wireless*, **13**(2), pp. 32–46.

21. Fu, W., Lopez, E.R., Rowe, W.S.T., Ghorbani, K., 2008. A Compact Broadband spiral antenna, school of electrical and computer engineering. In: *Proc. Microwave Asia-Pacific Conf.* (APMC'08). Hong Kong, 16–20 December 2008.

22. Lopez, W., Rowe, E., Ghorbani, W., 2010. A planar dual-arm equiangular spiral antenna. *IEEE Trans. Antennas Propag.*, **58**(5), pp. 1775–1779.

23. Lee, S., Lee, J., Joong, Y., 2011. Wideband thick-arm spiral antenna for ingestible capsules. *Microwave Opt. Technol. Lett.*, **53**(3), pp. 529–532.

24. Schreider, L., Begaud, X., Soiron, M., Perpere, B., 2004. Archimedean microstrip spiral antenna loaded by chip resistors inside substrate. In: *IEEE Int. Antennas and Propagation Society Symp.* Proc. Monterey, California, USA, 20–25 June 2004, pp. 1066–1069.

25. Eubanks, T., Chang, K., 2010. A Compact Parallel-Plane Perpendicular-Current Feed for a Modified Equiangular Spiral Antenna. *IEEE Trans. Antennas Propag.*, **58**(7), pp. 2193–2202.

26. Fu, W., Lopez, E. R., Scott, J., Rowe, W. S. T., Ghorbani, K., 2007. Broadband equiangular spiral antenna with embedded chip resistors. In: *Proc. Microwave Asia-Pacific Conf.* (APMC'07), Bangkok, Thailand, 11–14 December 2007.

27. Wang, G., Bavisi, A., Woods, W., Ding, H., Mina, E., 2011. A 77-GHz Marchand balun for antenna applications in BiCMOS technology. *Microwave Opt. Technol. Lett.*, **53**(3), pp. 664–666.

28. Salem, P., Wu, C., Yagoub, M.C.E., 2005. Novel ultra wideband printed balun design using the FEM and FDTD methods. In: *Int. Antennas and Propagation Society Symp*. (COPOL'05). Washington, DC, July 2005, pp. 643–646.

29. Hung, K. F., Lin, Y. C., 2006. Simulation of Single-Arm Fractional Spiral Antennas for Millimeter Wave Applications. In: *Proc. Int. Antennas and Propagation Society Symp.* IEEE, Albuquerque, NM, 9–14 July 2006, P. 3697–3700.

30. Bellion, A., Le Meins, C., Julien-Vergonjanne, A., Monediere, T., 2008. A New Compact Dually Polarized Direction Finding Antenna on the UHF Band. In: *Proc. Int. Antennas and Propagation Symp. and USNC/URSI National Radio Science Meeting* (APSURSI). San Diego, California, 5–15 July 2008.

31. Sarkis, R., Mani, F. and Craeye, C., 2008. Amplitude and Phase Correction of the Radiation Pattern in Compact Planar Antenna Array for Direction Finding Applications. In: *Proc. Int. Antennas and Propagation Symp. and USNC/URSI National Radio Science Meeting* (APSURSI). San Diego, California, 5–15 July 2008.

32. Lee, J., Chu, R., 1989. Aperture matching of a dielectric loaded circular waveguide element array. *IEEE Trans. Antennas Propag.*, **37**(3), pp. 395–399.

33. Coman, C.I., Lager, I.E., Ligthart, L.P., 2004. Optimization of linear sparse array antennas consisting of electromagnetically coupled apertures. In: *Proc. European Radar Conf.* (EuMW'2004). The Netherlands, Amsterdam, 11–15 October 2004, pp. 302–304.

34. Sharma, S., Shafai, L., 2005. Beam Focusing Properties of Circular Monopole Array Antenna on a Finite Ground Plane. *IEEE Trans. Antennas Propag.*, **53**(10), pp. 3406–3409.

35. Bolomey, J.-C., Gardiol, F.E., 2001. *Engineering application of the modulated scatterer technique*. Boston–L.: Artech House.

36. Baudry, D., 2007. Applications of the Near-Field Techniques in EMC Investigations. *IEEE Trans Electromagn. Compat.*, **49**(3), pp. 485–493.

37. Bhardwaj, S., Rahmat-Samii, Y., 2014. Revisiting the Generation of Cross-Polarization in Rectangular Patch Antennas: A Near-Field Approach. *IEEE Antennas Propag. Mag.*, **56**(1), pp. 14–38.

38. Sirenko, Y.K., 2002. Exact 'absorbing' conditions in outer initial boundary-value problems of electrodynamics of nonsinusoidal waves. Part 1: Fundamental theoretical statements. *Telecommunications and Radio Engineering*, **57**(10,11), pp. 1–20.

39. Ivanchenko, D., Ivanchenko, I., Korolev, A., Popenko, N., 2002. Experimental studies of X-band leaky-wave antenna performances. *Microwave Opt. Technol. Lett.*, **35**(4), pp. 277–281.

40. Andrenko, A., Ivanchenko, I., Ivanchenko, D., Karelin, S., Korolev, A., Laz'ko, E., Popenko, N., 2006. Active Broad X-Band Circular Patch Antenna. *IEEE Antennas Wirel. Propag. Lett.*, **5**, pp. 529–533.

41. Ivanchenko, I., Khruslov, M., Popenko, N., 2012. Diffraction Effects in the Cylindrical Monopole and Dielectric Disk Antennas. *Radio phys. radio astron.*, **17**(1), pp. 81–88.

42. Ivanchenko, I., Popenko, N., Khruslov, M., 2012. Effect of diffraction-coupled Apertures on the monopole antenna performance. *Radioelectronics & Informatics*, **4**, pp. 4–8.

43. Ivanchenko, I., Popenko, N., Khruslov, M., Chernobrovkin, R., 2008. Beamforming features of the grounded dielectric substrate based X-band monopole antenna. *Radioelectronics & Informatics*, **4**, pp. 4–10.

44. Ivanchenko, I.V., Popenko, N.A., Khruslov, M.M., 2015. *Small aperture axial-symmetric microwave radiators*. LAP LAMBERT Academic Publishing (in Russia).

45. Ivanchenko, I.V., Popenko, N.A., 2013**.** Investigation of electromagnetic field distributions as a method for studying the characteristics of electrodynamic structures. *Fizicheskie osnovy priborostroeniya*, **2**(1), pp. 18–33 (in Russian).

46. Radionov, S., Khruslov, M., Ivanchenko, I., Popenko, N., 2014. Beamforming by the metalized dielectric disk with off-axis excitation. *Telecommunications and Radio Engineering*, **73**(15), pp. 1327–1337.

47. Radionov, S.A., Ivanchenko, I.V., Popenko, N.A., Khruslov, M.M., 2015. *Dielectric disk antenna.* Ukraine. Pat. 97247 (in Russian).

48. Radionov, S. A., Ivanchenko, I. V., Popenko, N. A., 2014. Bimodal dielectric disk antenna. In: *Proc. 20th Int. Conf. Microwaves, Radar and Wireless Communications* (MIKON 2014). Gdansk, Poland, 16–18 June 2014, pp. 116–118.

49. Ivanchenko, I., Ivanchenko, D., Korolev, A., Popenko, N., Radionov, S., 2008. Mobile X-band direction finder. *Radioelectronics & Informatics,* **4**, pp. 11–15.

50. Radionov, S., Ivanchenko, I., Korolev, A., Popenko, N., 2008. Broadband SHF Direction-Finder. *Radioengineering*, **17**(2), pp. 61–65.

51. Radionov, S.A., Ivanchenko, I.V., Khruslov, M.M., Korolev A.M., Popenko, N.A., 2010. New X-Band Mobile Direction Finder. In: *Microwave and Millimeter Wave Technologies: from Photonic Bandgap Devices to Antenna and Applications*. Ed. by Prof. I. Minin. Publ. INTECH, pp. 273–288.

52. Ivanchenko, I.V., Popenko, N.A., Khruslov, M.M., Shestopalov, Yu.V., Rönnow, D., 2016. Combined System of the Microstrip Antennas with Different Frequencies. In: *Proc. 22nd Int. Conf. Applied Electromagnetics and Communications* (ICECom 2016). Dubrovnik, Chroatia, 19–21 September 2016.

53. Chernobrovkin, R., Ivanchenko, I., Pischikov, V., Popenko, N., 2012. UWB equiangular spiral antenna for 7.5–40GHz. *Microwave and optical technology letters*, **54**(9), pp. 2190–2194.

54. Chernobrovkin, R., Ivanchenko, D., Ivanchenko, I., Popenko, N., Pishikov, V., 2014. A compact broadband spiral antenna for millimeter wave applications. *Microwave and optical technology letters,* **56**(2), pp. 293–297.

55. Khruslov, M., 2013. K band Antennas Conjugated with a Metal Waveguide. *Radioelectronics & Informatics*, **1**, pp. 8–11.

56. Ivanchenko, I., Khruslov, M., Plakhtiy, V., Popenko, N., Rönnow, D., 2016. X-band aperture antenna with the hybrid dielectric insert. *Progress in Electromagnetics Research C*, **61**, pp. 27–35.

57. Chernobrovkin, R., Ivanchenko, I., Popenko, N., 2007. A Novel V-band Antenna for Nondestructive Testing Techniques. *Microwave Opt. Technol. Lett.*, **49**(7), pp. 1732–1735.

58. Chernobrovkin, R., Ivanchenko, I., Ligthart, L., Korolev, A., Popenko, N., 2008. Wide-angle X-band antenna array with novel radiating elements. *Radioengineering*, **17**(2), pp. 72–76.

59. Ivanchenko, I., Popenko, N., Pishchikov, V., Khruslov, M., Chernobrovkin, R., 2014. The features of radiation formation by the small-aperture SHF antennas. *Telecommunications and Radio Engineering*, **73**(2), pp. 135–150.

Received 25.02.2019

И. Иванченко [1], Н. Попенко [1], М. Хруслов [1,2], Р. Чернобровкин [1], С. Радионов [1], В. Пищиков [1]

[1]Институт радиофизики и электроники им. А.Я. Усикова НАН Украины
12, ул. Акад. Проскуры, Харьков, 61085, Украина
[2]Харьковский национальный университет имени В. Н. Каразина
4, пл. Свободы, Харьков, 61022, Украина

РАЗВИТИЕ КОНЦЕПЦИИ БЛИЖНИХ ПОЛЕЙ ПРИ РАЗРАБОТКЕ ЭФФЕКТИВНЫХ МАЛОАПЕРТУРНЫХ СВЧ-АНТЕНН

Предмет и цель работы. Статья посвящена обзору публикаций авторов по исследованию эффективных малоразмерных одиночных излучателей различных типов с применением технологии ближних полей.

Методы и методология работы. Алгоритм исследования состоит в проведении с помощью программных пакетов численного моделирования предлагаемых антенных дизайнов, создании соответствующих физических прототипов, а также сравнении результатов численных и натурных экспериментов по изучению таких характеристик излучателя, как полоса пропускания, диаграмма направленности, коэффициенты усиления и эллиптичности. Детальный анализ пространственных распределений ближних полей дает необходимую информацию для дальнейшей оптимизации характеристик антенн.

Результаты работы. Систематизированы и проанализированы характеристики различных модификаций монопольных, дисковых, апертурных, микрополосковых и спиральных антенн с рекордными характеристиками, а также показана возможность их применения в компактном мобильном СВЧ-пеленгаторе и нелинейном локаторе. Результаты исследования дифракционной связи единичных апертурных излучателей с привлечением развитых методов регистрации пространственных распределений ближних электромагнитных полей использованы при создании лабораторного макета антенной решетки.

Заключение. Приведен обзор результатов исследований малоразмерных СВЧ-антенн различных типов за последнее десятилетие. Продемонстрирована эффективность использования информации о пространственном распределении

полей в индуктивной и волновой зонах излучающих апертур при разработке и последующей оптимизации основных характеристик как одиночных оригинальных излучателей, так и антенных решеток на их основе.

Ключевые слова: антенна, антенная решетка, полоса пропускания, ближнее поле, диаграмма направленности.

I. Іванченко[1]*, Н. Попенко*[1]*, М. Хруслов*[1,2]*, Р. Чернобровкін*[1]*, С. Радіонов*[1]*, В. Піщіков*[1]

[1]Інститут радіофізики та електроніки ім. О.Я. Усикова НАН України
  12, вул. Акад. Проскури, 61085, Україна
[2]Харківський національний університет имені В.Н. Каразіна
  4, пл. Свободи, Харків, 61022, Україна

РОЗВИТОК КОНЦЕПЦІЇ БЛИЖНІХ ПОЛІВ ПРИ РОЗРОБЛЕННІ ЕФЕКТИВНИХ МАЛОАПЕРТУРНИХ НВЧ-АНТЕН

Предмет і мета роботи. Статтю присвячено огляду публікацій авторів з дослідження ефективних малорозмірних одиночних випромінювачів різних типів із застосуванням технології ближніх полів.

Методи і методологія роботи. Алгоритм дослідження полягає в проведенні за допомогою програмних пакетів чисельного моделювання пропонованих антенних дизайнів, створенні відповідних фізичних прототипів, а також порівнянні результатів чисельних і натурних експериментів з дослідження таких характеристик випромінювача, як смуга пропускання, діаграма направленості, коефіцієнти посилення та еліптичності. Детальний аналіз просторових розподілів ближніх полів дає необхідну інформацію для подальшої оптимізації характеристик антен.

Результати роботи. Систематизовано та проаналізовано характеристики різних модифікацій монопольних, дискових, апертурних, мікросмужкових і спіральних антен з рекордними характеристиками, а також показано можливість їх застосування в компактному мобільному НВЧ-пеленгаторі і нелінійному локаторі. Результати дослідження дифракційного зв'язку одиничних апертурних випромінювачів із залученням розвинених методів реєстрації просторових розподілів ближніх електромагнітних полів використано при створенні лабораторного макета антенної решітки.

Висновок. Наведено огляд результатів досліджень малорозмірних НВЧ-антен різних типів за останнє десятиліття. Продемонстровано ефективність використання інформації про просторовий розподіл полів у індуктивній і хвильовій зонах випромінюючих апертур при розробці та подальшій оптимізації основних характеристик як одиночних оригінальних випромінювачів, так і антенних решіток на їх основі.

Ключові слова: антена, антенна решітка, смуга пропускання, ближнє поле, діаграма направленості.